



CHORUS

This is the accepted manuscript made available via CHORUS. The article has been published as:

Neutron spin resonance as a probe of Fermi surface nesting and superconducting gap symmetry in

$\text{Ba}_{0.67}\text{K}_{0.33}(\text{Fe}_{1-x}\text{Co}_x)_2\text{As}_2$

Rui Zhang, Weiyi Wang, Thomas A. Maier, Meng Wang, Matthew B. Stone, Songxue Chi, Barry Winn, and Pengcheng Dai

Phys. Rev. B **98**, 060502 — Published 30 August 2018

DOI: [10.1103/PhysRevB.98.060502](https://doi.org/10.1103/PhysRevB.98.060502)

Neutron spin resonance as a probe of Fermi surface nesting and superconducting gap symmetry in $\text{Ba}_{0.67}\text{K}_{0.33}(\text{Fe}_{1-x}\text{Co}_x)_2\text{As}_2$

Rui Zhang,¹ Weiyi Wang,¹ Thomas A. Maier,² Meng Wang,³ Matthew B. Stone,⁴ Songxue Chi,⁴ Barry Winn,⁴ and Pengcheng Dai^{1,*}

¹*Department of Physics and Astronomy, Rice University, Houston, Texas 77005, USA*

²*Computer Science and Mathematics Division and Center for Nanophase Materials Sciences, Oak Ridge National Laboratory, Oak Ridge, Tennessee 37831-6494, USA*

³*School of Physics, Sun Yat-Sen University, Guangzhou 510275, China*

⁴*Neutron Scattering Division, Oak Ridge National Laboratory, Oak Ridge, Tennessee 37831, USA*

We use inelastic neutron scattering to study energy and wave vector dependence of the superconductivity-induced resonance in hole-doped $\text{Ba}_{0.67}\text{K}_{0.33}(\text{Fe}_{1-x}\text{Co}_x)_2\text{As}_2$ ($x = 0, 0.08$ with $T_c \approx 37, 28$ K, respectively). In previous work on electron-doped $\text{Ba}(\text{Fe}_{0.963}\text{Ni}_{0.037})_2\text{As}_2$ ($T_N = 26$ K and $T_c = 17$ K), the resonance is found to peak sharply at the antiferromagnetic (AF) ordering wave vector \mathbf{Q}_{AF} along the longitudinal direction, but disperses upwards away from \mathbf{Q}_{AF} along the transverse direction [Kim *et al.*, Phys. Rev. Lett. **110**, 177002 (2013)]. For hole doped $x = 0, 0.08$ without AF order, we find that the resonance displays ring-like upward dispersion away from \mathbf{Q}_{AF} along both the longitudinal and transverse directions. By comparing these results with calculations using the random phase approximation, we conclude that the dispersive resonance is a direct signature of isotropic superconducting gaps arising from nested hole-electron Fermi surfaces.

Understanding the interaction between magnetism and unconventional superconductivity continues to be an important topic in modern condensed matter physics¹⁻⁴. In copper and iron-based high-transition-temperature (high- T_c) superconductors, the parent compounds are long-range ordered antiferromagnets and superconductivity arises from electron or hole-doping to the parent compounds¹⁻³. Although static antiferromagnetic (AF) order in the parent compounds is gradually suppressed with increasing doping, dynamic spin correlations (excitations) remain and inelastic neutron scattering (INS) experiments have identified a ubiquitous collective spin excitation mode, termed neutron spin resonance, that occurs below T_c with a temperature-dependence similar to the superconducting order parameter^{5,6,9-14}. Moreover, the energy of the resonance has been associated with T_c or superconducting gap size Δ ¹⁵⁻¹⁸, thus establishing its direct connection with superconductivity. For hole-doped copper oxide superconductors such as $\text{YBa}_2\text{Cu}_3\text{O}_{6+x}$, the resonance, obtained by subtracting the normal-state spin excitations from those in the superconducting state, displays predominantly a downward dispersion away from the in-plane AF ordering wave vector $\mathbf{Q}_{\text{AF}} = (1/2, 1/2)$ of the proximate tetragonal phase¹⁹⁻²². In the case of undoped iron pnictides, the AF order occurs in the orthorhombic lattice with spins aligned anti-parallel along the orthorhombic a_o axis (H direction in reciprocal space) and parallel along the b_o axis (K direction) at the in-plane wave vector at $\mathbf{Q}_{\text{AF}} = (1, 0)$ ³. Here, the resonance for electron-underdoped iron pnictide $\text{BaFe}_{1.926}\text{Ni}_{0.074}\text{As}_2$ with co-existing AF order and superconductivity²³ is centered around \mathbf{Q}_{AF} along the H (longitudinal) direction but has an upward spin-wave-like dispersion along the K (transverse) direction²⁴. Finally, for heavy Fermion superconductor CeCoIn_5 ⁴, the resonance exhibits a spin-wave ring like upward dispersion^{25,26} reminiscent of spin waves in

nonsuperconducting CeRhIn_5 ^{27,28}.

Although it is generally accepted that the presence of a resonance is a signature of unconventional superconductors¹, there is no consensus on its microscopic origin. The most common interpretation of the resonance is that it is a spin-exciton, arising from particle-hole excitations involving momentum states near the Fermi surfaces that possess opposite signs of the d -wave⁶⁻⁸ or s^\pm -wave²⁹ superconducting order parameter. For $d_{x^2-y^2}$ -wave superconductors such as copper oxides¹ and CeCoIn_5 ⁴, the resonance is expected to show a downward dispersion away from $\mathbf{Q}_{\text{AF}} = (1/2, 1/2)$ of their parent compounds⁶. Therefore, the surprising observation of a spin-wave ring like upward dispersion of the resonance in CeCoIn_5 ²⁶ suggests that the mode is a magnon-like excitation revealed in the superconducting state due to reduced hybridization between f electrons and conduction electrons, and not an indication of a sign reversed order parameter³⁰. For iron pnictide superconductors [Fig. 1(a)], the resonance is generally believed to be a spin exciton arising from sign-reversed quasiparticle excitations between the hole and electron Fermi surfaces located at Γ and X/Y points in reciprocal space, respectively [Fig. 1(e)]²⁹. Although the observation of a transverse upward spin-wave-like dispersive resonance in superconducting $\text{BaFe}_{1.926}\text{Ni}_{0.074}\text{As}_2$ is different from the downward dispersion of the mode in $\text{YBa}_2\text{Cu}_3\text{O}_{6+x}$, it has been argued that the mode is a spin exciton arising from isotropic s^\pm superconducting gaps at Γ and X/Y points and its coupling with the normal state spin fluctuations via

$$\Omega_{\mathbf{q}} = \sqrt{\Omega_0^2 + c_{res,\mathbf{q}}^2} \quad (1)$$

, where Ω_0 is the resonance energy, $c_{res,\mathbf{q}} = \Omega_0 \xi_{\mathbf{q}}$ is the velocity of the resonance and its anisotropy in momentum (\mathbf{q}) space is due to the anisotropy in the normal

state spin-spin correlation length $\xi_{\mathbf{q}}$ ^{24,31,32}. However, spin waves from static AF order coexisting with superconductivity in $\text{BaFe}_{1.926}\text{Ni}_{0.074}\text{As}_2$ may complicate such interpretation.

If the resonance in iron pnictide superconductors is indeed a spin exciton without related to spin waves from static AF order, one would expect that modifying the wave vector dependence of the normal state spin fluctuations should affect the dispersion of the resonance, as the former is directly associated with shapes of the hole and electron Fermi surfaces in reciprocal space³³. From previous work on electron and hole-doped BaFe_2As_2 , we know that the low-energy (< 40 meV) normal state spin fluctuations change from transversely elongated for electron-doped $\text{BaFe}_{2-x}\text{Ni}_x\text{As}_2$ ³⁴ to longitudinally elongated for hole doped $\text{Ba}_{0.67}\text{K}_{0.33}\text{Fe}_2\text{As}_2$, while the high-energy ($E \geq 50$ meV) spin fluctuations of these materials have similar transverse elongation^{35,36}. Therefore, it would be of great interests to study the dispersion of the resonance in $\text{Ba}_{0.67}\text{K}_{0.33}\text{Fe}_2\text{As}_2$ and its electron-doping effect in $\text{Ba}_{0.67}\text{K}_{0.33}(\text{Fe}_{1-x}\text{Co}_x)_2\text{As}_2$ [Fig. 1(a)] to test the spin exciton hypothesis^{37,38}.

In this paper, we use time-of-flight (TOF) INS experiments to study wave vector and energy dependence of the resonance in hole-doped $\text{Ba}_{0.67}\text{K}_{0.33}\text{Fe}_2\text{As}_2$ ($T_c = 38$ K) and its electron-compensated $\text{Ba}_{0.67}\text{K}_{0.33}(\text{Fe}_{0.92}\text{Co}_{0.08})_2\text{As}_2$ ($T_c = 28$ K) without static AF order, where Co and K doping levels are nominal [Fig. 1(a)]. We find that the resonance in $\text{Ba}_{0.67}\text{K}_{0.33}\text{Fe}_2\text{As}_2$ has a spin-wave ring-like dispersion extending more along the longitudinal (H) than the transverse (K) directions from \mathbf{Q}_{AF} [Fig. 2(a-c)]. Upon electron-doping to form $\text{Ba}_{0.67}\text{K}_{0.33}(\text{Fe}_{0.92}\text{Co}_{0.08})_2\text{As}_2$ with reduced T_c , the dispersion along the longitudinal direction narrows [Figs. 1(c) and 1(d)]. These results can be understood as arising from isotropic superconducting gaps in nested hole and electron Fermi surfaces within the BCS theory in the random phase approximation (RPA) calculation of the spin exciton model^{39,40}. Our results thus establish that the spin-wave-like dispersion of the resonance in iron pnictides is a spin exciton of a nested hole and electron Fermi surfaces.

We carried out INS experiments using the SEQUOIA spectrometer at the Spallation Neutron Source and the HB-3 triple-axis spectrometer in High Flux Isotope Reactor, both at Oak Ridge National Laboratory. For TOF INS experiment, we prepared 11 g of sizable $\text{Ba}_{0.67}\text{K}_{0.33}(\text{Fe}_{0.92}\text{Co}_{0.08})_2\text{As}_2$ single crystals and co-aligned them on aluminum plates³⁵. The $\text{Ba}_{0.67}\text{K}_{0.33}\text{Fe}_2\text{As}_2$ single crystals were previously measured³⁶. The TOF experiments used incident neutrons parallel to the c axis with incident energies of $E_i = 35, 80, \text{ and } 250$ meV with corresponding Fermi chopper frequency $\omega = 180, 420, 600$ Hz, respectively. We define $(H, K, L) = (q_x a/2\pi, q_y b/2\pi, q_z c/2\pi)$ using the orthorhombic lattice notation for the tetragonal lattice, where $a = b \approx 5.57$ Å, $c = 13.13$ Å. The experiments on HB-3 used a pyrolytic graphite monochromator, ana-

lyzer, and filter after the sample with fixed final energy $E_f = 14.7$ meV and collimators of $48'80'$ -sample- $40'240'$.

Figure 1(a) shows the electronic phase diagram of $\text{Ba}_{0.67}\text{K}_{0.33}(\text{Fe}_{1-x}\text{Co}_x)_2\text{As}_2$ as determined from our neutron diffraction experiments⁴¹. Consistent with earlier work^{37,38}, we see that Co-doping to $\text{Ba}_{0.67}\text{K}_{0.33}\text{Fe}_2\text{As}_2$ gradually suppresses superconductivity and induces long-range AF order for $x \geq 0.16$. To systematically investigate the Co-doping evolution of the resonance without complication of static AF order, we focus on $x = 0, 0.08$ samples [Fig. 1(a)]. Figure 1(b) summarizes the three dimensional (3D) dispersion of the resonance in $x = 0.08$, obtained by taking the temperature difference of spin excitation spectra between the superconducting state at $T = 5$ K and the normal state at $T = 40$ K. While the resonance first starts to emerge from $E = 5$ meV at $\mathbf{Q}_{\text{AF}} = (1, 0)$, it has strong in-plane dispersion along both the H and K directions, which leads to a ring of scattering in the (H, K) plane at $E = 18 \pm 1$ meV. These results are clearly different from electron-doped $\text{Ba}(\text{Fe}_{0.963}\text{Ni}_{0.037})_2\text{As}_2$ where the modes disperses only along the K direction²⁴.

To determine the Co-doping evolution of the resonance, we show in Figs. 1(c) and 1(d) the dispersions of the mode along the H -direction for $x = 0$ and 0.08 , respectively. Inspection of the figures reveals a clear narrowing of the width of the resonance with increasing x . These results are qualitatively consistent with expectations of hole and electron Fermi surface nesting, where Co-doping reduces the size of the hole pocket near Γ and increases the size of the electron pocket near the X/Y points [Figs. 1(e), and 1(f)]³.

Figure 2 summarizes the wave vector and energy dependence of spin excitations near the resonance energy in the normal and superconducting states of $x = 0, 0.08$ samples. For $x = 0$, spin excitations in the superconducting state are longitudinally elongated, with the longitudinal elongation increasing with increasing energy [Figs. 2(a)-2(c)]. In the normal state [Figs. 2(d)-2(f)], the in-plane spin excitations show less anisotropy from 15 meV [Fig 2(d)] up to 23 meV [Fig 2(f)]. For $x = 0.08$, while the normal state spin excitations are centered at $\mathbf{Q}_{\text{AF}} = (1, 0)$ for all measured energies [Figs. 2(j)-2(l)], progressive larger ring-like features appear at $E = 13 \pm 1, 17 \pm 1, \text{ and } 19 \pm 1$ meV [Figs. 2(g)-2(i)].

To understand the normal state spin excitations and their connection with the resonance, we fit the normal state spin excitations with a Fermi liquid model and find the in-plane two-dimensional (2D) correlation length $\xi_{\mathbf{q}}$ ^{24,41}. The anisotropic $\xi_{\mathbf{q}}$ can be used to estimate the resonance dispersion $\Omega_{\mathbf{q}}^2 = \Delta_{\mathbf{q}}\Gamma_{\mathbf{q}}(1 + \xi_{\mathbf{q}}^2\mathbf{q}^2)$, where $\Delta_{\mathbf{q}}$ is the \mathbf{q} -dependent superconducting gap and $\Gamma_{\mathbf{q}}$ is the \mathbf{q} -dependent Landau damping²⁴. Assuming an isotropic Landau damping and superconducting gap, the dispersion of the resonance mode is reduced to equation (1) with $c_{res,\mathbf{q}} = \Omega_0\xi_{\mathbf{q}}$, thus directly connects normal state spin correlation length (and its anisotropy) to the resonance dispersion. Although such a picture can quali-

tatively capture the ring-like upward dispersion of the resonance, it cannot explain the change in the longitudinal elongation of the spin excitations from the normal to the superconducting state [Figs. 2(a)-2(f)]³⁶.

By computing the differences between the normal ($T = 45$ K) and superconducting ($T = 5$ K) state measurements⁶, Figures 3(a)-3(c) show in-plane \mathbf{q} -dependence of the resonance at energies of $E = 12 \pm 1$, 15 ± 1 , and 21 ± 2 meV, respectively, for $x = 0$. At $E = 12 \pm 1$ meV, the resonance is a longitudinally elongated ellipse centered at $\mathbf{Q}_{AF} = (1, 0)$. On moving to $E = 15 \pm 1$ meV, the ellipse becomes slightly larger but is still centered at \mathbf{Q}_{AF} . Further increasing energies to $E = 21 \pm 2$, we find elliptical ring-like scattering dispersing away from \mathbf{Q}_{AF} . Figures 3(g)-3(i) summarize similarly subtracted data for $x = 0.08$, which reveal a clear ring-like resonance at energies $E = 15 \pm 1$, and 17 ± 1 meV. Compared with $x = 0$, the resonance has ring-like scattering in $x = 0.08$ but is more isotropic in reciprocal space along the H and K directions.

Although Figures 1-3 have shown the dispersive ring-like feature of the resonance in $x = 0, 0.08$ samples, the mode has a rather broad energy width that may be related to inhomogeneous superconductivity⁶. It is therefore important to establish temperature dependence of the commensurate and ring-like response below T_c , and determine if the ring-like feature also responds to superconductivity and is related to the superconducting gap function. Figures 4(a)-4(d) show the 2D images of the resonance at 15 K and 25 K for the $x = 0.08$ sample. The corresponding one-dimensional (1D) cuts are shown in Figs. 4(e)-4(h). While intensity of the resonance at probed energies decreases with increasing temperature and vanishes at T_c , the wave vector dependence of the mode and the ring-like feature have no visible temperature dependence. Figure 4(i) shows temperature dependence of the integrated intensity of the resonance at $E = 15 \pm 1$, 20 ± 1 , and 12 meV. At all probed energies, temperature dependence of the resonance behave identically, suggesting that they are related to the superconducting gap function.

Having established the wave vector and Co-doping dependence of the resonance dispersion and normal state spin excitations in $\text{Ba}_{0.67}\text{K}_{0.33}(\text{Fe}_{1-x}\text{Co}_x)_2\text{As}_2$, we now test if the dispersion of the mode is well described by the spin exciton model of eq. (1)²⁴. To do this, we first fitted the 2D normal state spin excitations in Figs. 2(d)-2(f) and 2(j)-2(l) with $\xi_{\mathbf{q}}$ ^{24,41}, the outcome was then used to fit the data in the superconducting state and obtain $c_{res,\mathbf{q}}$ along different directions. For $x = 0$, we find $c_{res,H} \approx 154$ and $c_{res,K} \approx 169$ meVÅ. Fitting the actual dispersion curves of the resonance in Figs. 1(c) and 3(a)-3(c) with a linear dispersion yields $c_{res,H}(\text{exp}) \approx 65$ and $c_{res,K}(\text{exp}) \approx 84$ meVÅ. Similarly, we find $c_{res,H} \approx 126$ and $c_{res,K} \approx 141$ meVÅ, and $c_{res,H}(\text{exp}) \approx 78$ and $c_{res,K}(\text{exp}) \approx 87$ meVÅ for $x = 0.08$. The effect of increasing Co-doping from $x = 0$ to $x = 0.08$ is to increase $c_{res,H}(\text{exp})$, while $c_{res,K}(\text{exp})$ remains virtually

unchanged.

To quantitatively understand the experimental results, we have used a BCS/RPA approximation³⁹ to calculate the magnetic susceptibility $\chi''(\mathbf{Q}_{AF}, E)$ from a 3D tight-binding five-orbital Hubbard-Hund model that describes the electronic structure of BaFe_2As_2 ⁴⁰. The effect of doping by K and Co substitution is estimated by a rigid band shift. Specifically, we use a filling of $\langle n \rangle = 5.915$ corresponding to a hole doping of 8.5% to model the $x = 0.08$ system. For the superconducting gap, we have used an isotropic s^\pm gap with $\Delta = 8$ meV on the Fermi surface hole cylinders around the zone center and $\Delta = -8$ meV on the electron cylinders around the zone corner. The interaction matrix in orbital space used in the RPA calculation contains on-site matrix elements for the intra-orbital and inter-orbital Coulomb repulsions U and U' , and for the Hund's-rule coupling and pair-hopping terms J and J' , respectively. Here, we have used spin-rotationally invariant parameters $J = J' = U/4$ and $U' = U/2$ with $U = 0.77$ eV.

For these parameters, we obtain a resonance in $\chi''(\mathbf{Q}_{AF}, E)$ at $\mathbf{Q}_{AF} = (1, 0)$ and $E = 10$ meV. Moving away from \mathbf{Q}_{AF} , the resonance disperses upward resulting in a ring-like feature in constant energy scans that is slightly elongated along the longitudinal direction similar to what is observed in the experimental data. At energies above ~ 17 meV, the ring-like excitations disappear and change into a broad blob centered at $\mathbf{Q}_{AF} = (1, 0)$. Figures 3(d)-3(f) and 3(j)-3(l) summarize the Co-doping and energy dependence of the resonance from the RPA calculation. We see that the RPA calculation with isotropic superconducting gap can describe very well the energy and doping evolution of the resonance, further confirming the spin exciton nature of the resonance although details of the dispersion calculated from RPA still differ somewhat from the experiments.

In summary, we have used TOF INS to study the wave vector-energy dispersion of the resonance in $\text{Ba}_{0.67}\text{K}_{0.33}(\text{Fe}_{1-x}\text{Co}_x)_2\text{As}_2$ with $x = 0, 0.08$. Compared with electron-doped underdoped superconducting $\text{Ba}(\text{Fe}_{0.963}\text{Ni}_{0.037})_2\text{As}_2$, where the resonance displays a strong transverse dispersion but centered at \mathbf{Q}_{AF} along the longitudinal direction²⁴, the resonance in $\text{Ba}_{0.67}\text{K}_{0.33}(\text{Fe}_{1-x}\text{Co}_x)_2\text{As}_2$ has ring-like dispersion that follows the evolution of the Fermi surface nesting with increasing Co-doping. These results are consistent with expectations of a spin exciton model with BCS/RPA approximation, indicating that the mode arises from particle-hole excitations involving momentum states near the sign-reversed electron-hole Fermi surfaces.

The neutron-scattering work at Rice University was supported by the US NSF Grant No. DMR-1700081 (P.D.). The single-crystal synthesis work was supported by the Robert A. Welch Foundation Grant No. C-1839 (P.D.). T.A.M was supported by the U.S. Department of Energy, Office of Basic Energy Sciences, Materials Sciences and Engineering Division. This research used resources at the High Flux Isotope Reactor and Spallation

- * Electronic address: pdai@rice.edu
- ¹ D. J. Scalapino, *Rev. Mod. Phys.* **84**, 1383 (2012).
 - ² B. Keimer, S. A. Kivelson, M. R. Norman, S. Uchida, J. Zaanen, *Nature (London)* **518**, 179-186 (2015).
 - ³ P. C. Dai, *Rev. Mod. Phys.* **87**, 855 (2015).
 - ⁴ J. D. Thompson and Z. Fisk, *J. Phys. Soc. Jpn.* **81**, 011002 (2012).
 - ⁵ J. Rossat-Mignod, L. P. Regnault, C. Vettier, P. Bourges, P. Burllet, J. Bossy, J. Y. Henry, and G. Lapertot, *Phys. C* **185-189**, 86 (1991).
 - ⁶ M. Eschrig, *Adv. Phys.* **55**, 47183 (2006).
 - ⁷ A. Abanov and A. V. Chubukov *Phys. Rev. Lett.* **83**, 1652 (1999).
 - ⁸ A.V. Chubukov, B. Janko, and O. Tchernyshyov, *Phys. Rev. B* **63**, 180507(2001).
 - ⁹ A. D. Christianson, E. A. Goremychkin, R. Osborn, S. Rosenkranz, M. D. Lumsden, C. D. Malliakas, I. S. Todorov, H. Claus, D. Y. Chung, M. G. Kanatzidis, R. I. Bewley, and T. Guidi, *Nature* **456**, 930 (2008).
 - ¹⁰ M. D. Lumsden, A. D. Christianson, D. Parshall, M. B. Stone, S. E. Nagler, G. J. MacDougall, H. A. Mook, K. Lokshin, T. Egami, D. L. Abernathy, E. A. Goremychkin, R. Osborn, M. A. McGuire, A. S. Sefat, R. Jin, B. C. Sales, and D. Mandrus, *Phys. Rev. Lett.* **102**, 107005 (2009).
 - ¹¹ S. Chi, A. Schneidewind, J. Zhao, L. W. Harriger, L. J. Li, Y. K. Luo, G. H. Cao, Z. A. Xu, M. Loewenhaupt, J. P. Hu, and P. C. Dai, *Phys. Rev. Lett.* **102**, 107006 (2009).
 - ¹² D. S. Inosov, J. T. Park, P. Bourges, D. L. Sun, Y. Sidis, A. Schneidewind, K. Hradil, D. Haug, C. T. Lin, B. Keimer, and V. Hinkov, *Nat. Phys.* **6**, 178 (2010).
 - ¹³ C. Zhang, R. Yu, Y. Su, Y. Song, M. Wang, G. Tan, T. Egami, J. A. Fernandez-Beca, E. Faulhaber, Q. Si, and P. C. Dai, *Phys. Rev. Lett.* **111**, 207002 (2013).
 - ¹⁴ C. Stock, C. Broholm, J. Hudis, H. J. Kang, and C. Petrovic, *Phys. Rev. Lett.* **100**, 087001 (2008).
 - ¹⁵ S. D. Wilson, P. C. Dai, S. L. Li, S. X. Chi, H. J. Kang, and J. W. Lynn, *Nature* **442**, 59 (2006).
 - ¹⁶ D. S. Inosov, J. T. Park, A. Charnukha, Y. Li, A. V. Boris, B. Keimer, and V. Hinkov, *Phys. Rev. B* **83**, 214520 (2011).
 - ¹⁷ G. Yu, Y. Li, E. M. Motoyama, and M. Greven, *Nat. Phys.* **5**, 873 (2009).
 - ¹⁸ Qisi Wang, J. T. Park, Yu Feng, Yao Shen, Yiqing Hao, Bingying Pan, J.W. Lynn, A. Ivanov, Songxue Chi, M. Matsuda, Huibo Cao, R. J. Birgeneau, D. V. Efremov, and Jun Zhao, *Phys. Rev. Lett.* **116**, 197004 (2016).
 - ¹⁹ P. Bourges, Y. Sidis, H. F. Fong, L. P. Regnault, J. Bossy, A. Ivanov, B. Keimer, *Science* **288**, 1234 (2000).
 - ²⁰ P. C. Dai, H. A. Mook, R. D. Hunt, and F. Doğan, *Phys. Rev. B* **63**, 054525 (2001).
 - ²¹ D. Reznik, P. Bourges, L. Pintschovius, Y. Endoh, Y. Sidis, T. Masui, and S. Tajima, *Phys. Rev. Lett.* **93**, 207003 (2004).
 - ²² S. M. Hayden, H. A. Mook, P. C. Dai, T. G. Perring, and F. Doğan, *Nature* **429**, 531 (2004).
 - ²³ X. Lu, H. Gretarsson, R. Zhang, X. Liu, H. Luo, W. Tian, M. Laver, Z. Yamani, Y. -J. Kim, A. H. Nevidomskyy, Q. Si, and P. Dai, *Phys. Rev. Lett.* **110**, 257001 (2013).
 - ²⁴ M. G. Kim, G. S. Tucker, D. K. Pratt, S. Ran, A. Thaler, A. D. Christianson, K. Marty, S. Calder, A. Podlesnyak, S. L. Bud'ko, P. C. Canfield, A. Kreyssig, A. I. Goldman, and R. J. McQueeney, *Phys. Rev. Lett.* **110**, 177002 (2013).
 - ²⁵ S. Raymond and G. Lapertot, *Phys. Rev. Lett.* **115**, 037001 (2015).
 - ²⁶ Yu Song, John Van Dyke, I. K. Lum, B. D. White, Sooyoung Jang, Duygu Yazici, L. Shu, A. Schneidewind, Petr Čermák, Y. Qiu, M. B. Maple, Dirk K. Morr, and P. C. Dai, *Nat. Comm.* **7**, 12774 (2016).
 - ²⁷ Pinaki Das, S.-Z. Lin, N.J. Ghimire, K. Huang, F. Ronning, E.D. Bauer, J.D. Thompson, C.D. Batista, G. Ehlers, and M. Janoschek, *Phys. Rev. Lett.* **113**, 246403 (2014).
 - ²⁸ C. Stock, J.A. Rodriguez-Rivera, K. Schmalzl, E.E. Rodriguez, A. Stunault, and C. Petrovic, *Phys. Rev. Lett.* **114**, 247005 (2015).
 - ²⁹ P. J. Hirschfeld, M. M. Korshunov, and I. I. Mazin, *Rep. Prog. Phys.* **74**, 124508 (2011).
 - ³⁰ A. V. Chubukov and L. P. Gor'kov, *Phys. Rev. Lett.* **101**, 147004 (2008).
 - ³¹ G. S. Tucker, R.M. Fernandes, H.-F. Li, V. Thampy, N. Ni, D. L. Abernathy, S. L. Budko, P. C. Canfield, D. Vaknin, J. Schmalian, and R. J. McQueeney, *Phys. Rev. B* **86**, 024505 (2012).
 - ³² H. Q. Luo, Z. Yamani, Y. C. Chen, X. Y. Lu, M. Wang, S. L. Li, T. A. Maier, S. Danilkin, D. T. Adroja and P. C. Dai, *Phys. Rev. B* **66**, 024508(2012).
 - ³³ J. H. Zhang, R. Sknepnek, and J. Schmalian, *Phys. Rev. B* **82**, 134527 (2010).
 - ³⁴ Huiqian Luo, Xingye Lu, Rui Zhang, Meng Wang, E. A. Goremychkin, D. T. Adroja, Sergey Danilkin, Guochu Deng, Zahra Yamani, and Pengcheng Dai, *Phys. Rev. B* **88**, 144516 (2013).
 - ³⁵ C. L. Zhang, M. Wang, H. Q. Luo, M. Y. Wang, M. S. Liu, J. Zhao, D. L. Abernathy, T. A. Maier, Karol Marty, M. D. Lumsden, S. Chi, S. Chang, Jose A. Rodriguez-Rivera, J. W. Lynn, T. Xiang, J. P. Hu, and P. C. Dai, *Sci. Rep.* **1**, 115 (2011).
 - ³⁶ Meng Wang, Chenglin Zhang, Xingye Lu, Guotai Tan, Huiqian Luo, Yu Song, Miaoyin Wang, Xiaotian Zhang, E.A. Goremychkin, T.G. Perring, T.A. Maier, Zhiping Yin, Kristjan Haule, Gabriel Kotliar, and Pengcheng Dai, *Nat. Comm.* **4**, 2874 (2013).
 - ³⁷ J. Li, Y. F. Guo, S. B. Zhang, J. Yuan, Y. Tsujimoto, X. Wang, C. I. Sathish, Y. Sun, S. Yu, W. Yi, K. Yamaura, E. Takayama-Muromachiu, Y. Shirako, M. Akaogi, and H. Kontani, *Phys. Rev. B* **85**, 214509 (2012)
 - ³⁸ T. Goltz, V. Zinth, D. Johrendt, H. Rosner, G. Pascua, H. Luetkens, P. Materne, and H-H. Klauss, *Phys. Rev. B* **89**, 144511 (2014).
 - ³⁹ T. Maier and D. Scalapino, *Phys. Rev. B* **78**, 020514 (2008).
 - ⁴⁰ S. Graser, A. F. Kemper, T. A. Maier, H. P. Cheng, P. J. Hirschfeld, and D. J. Scalapino, *Phys. Rev. B* **81**, 214503 (2010).
 - ⁴¹ For detailed data analysis and additional transport results, see supplementary material.

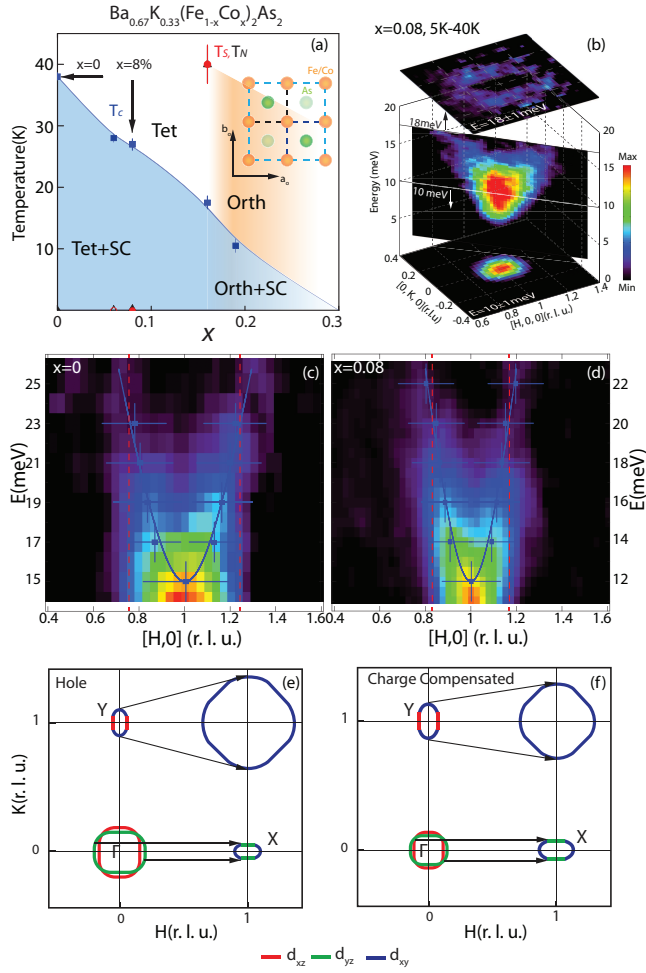


FIG. 1: (a) Electronic phase diagram of $\text{Ba}_{0.67}\text{K}_{0.33}(\text{Fe}_{1-x}\text{Co}_x)_2\text{As}_2$, black arrows indicate the Co-doping samples reported in this work. Blue squares, red triangles, black squares represent T_c , T_s , T_N respectively. (b) The 3D plot of the resonance dispersion of the $x = 0.08$ sample in reciprocal space after correcting the Bose population factor. The orange area marks possible long range AF ordered phase induced by Co-doping. The bottom and top slice shown in this plot are energy integrated at $E = 10 \pm 1$ and 18 ± 1 meV with $E_i = 35$ meV, respectively. (c,d) Constant wave vector slice of the resonance from 10 meV to 22 meV with $E_i = 35$ meV along the H direction for $x = 0$ and 0.08 , respectively. The slice is integrated from $-0.15 \leq K \leq 0.15$. The blue solid lines are fits of resonance dispersion using equation (1). The red dashed line indicates the width of the resonance dispersion at 8 meV above its initial energy. All scattering intensities in Figs. 1-4 are corrected by the magnetic form factor and Bose population factor. (e,f) Co-doping evolution of the Fermi surfaces from density functional theory calculation, where red, green, and blue indicate d_{xz} , d_{yz} , and d_{xy} orbitals.

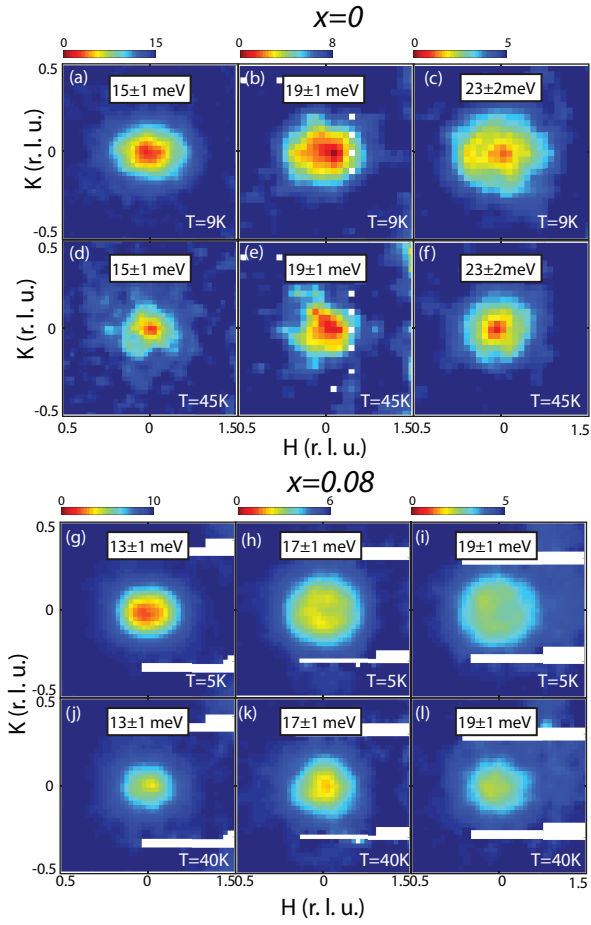


FIG. 2: The 2D images of spin excitations as a function of energy below and above T_c for $x = 0$ (a-f) and 0.08 (g-l). Cuts (a), (b), (d), (e), (g) (l) are taken with $E_i = 35$ meV and (c) and (f) are taken with $E_i = 70$ meV. The instrument energy resolutions for $E_i = 35$ meV and $E_i = 70$ meV are ~ 1.5 and 3.5 meV, respectively. The white areas in Figs. 2-4 are due to dead detectors.

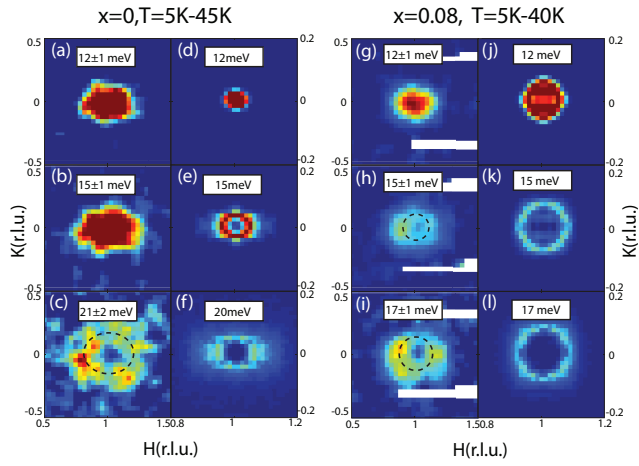


FIG. 3: Comparison of the dispersions of the resonance with BCS/RPA calculation. (a-c) Constant energy slice of spin resonance for $x = 0$. (d-f) Corresponding calculated images of the resonance from BCS/RPA theory. (g-i) Constant energy slice of spin resonance For $x = 0.08$. The dashed curves in the figures are expected spin wave dispersion using fits in Figs. 1(c), 1(d). (j-l) Corresponding images of the resonance from BCS/RPA theory.

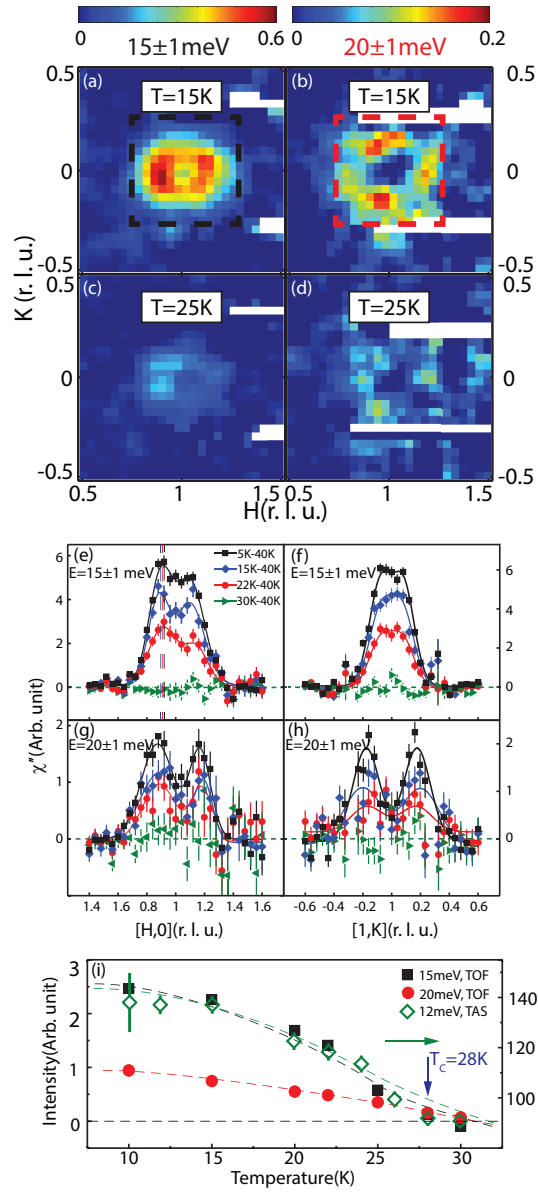


FIG. 4: Temperature dependence of the resonance at different energies for $x = 0.08$. (a,c) Temperature dependence of the resonance at $E = 15 \pm 1$. (b,d) Identical scans at $E = 20 \pm 1$ meV. (e-h) The corresponding 1D cuts along different directions. (i) Temperature dependence of the resonance at different energies, where T_c is marked by the vertical arrow. The integration area in $E = 15 \pm 1$ and 20 ± 1 meV correspond to black and red dashed boxes in (a).